# Microporosity and connections between pores in SBA-15 mesostructured silicas as a function of the temperature of synthesis

**Anne Galarneau,[a] Hélène Cambon,[a] Francesco Di Renzo,[a] Ryong Ryoo,[b] Minkee Choi[b] and François Fajula[a]**

[a] *Laboratoire de Matériaux Catalytiques et Catalyse en Chimie Organique, UMR 5618 ENSCM/CNRS, Ecole Nationale Supérieure de Chimie de Montpellier, 8 rue de l'Ecole Normale, 34296, Montpellier cedex 5, France. E-mail: galarne@cit.enscm.fr.*

[b] *National Creative Research Initiative Center fir Functional Materials, Department of Chemistry (School of Molecular Science-BK21), Korea Advanced Institute of Science and Technology, Daejeon 305-701, Korea. E-mail: rryoo@mail.kaist.ac.kr.*

***Received (in Montpellier, France) 26th July 2002, Accepted 2002th September 2002***
***First published as an Advance Article on the web 28th November 2002***

Imaging of the platinum replica of the porous structure and low-pressure argon adsorption allowed us to elucidate the complicated porous structure of SBA-15. These techniques enabled us to draw a coherent picture of the evolution of the SBA-15 precursor mesophase as a function of the synthesis temperature. TEM of the platinum replicas has been unable to show bridges between the structural mesopores of SBA-15 synthesized at low temperature, whereas mesoporous bridges are clearly observed for samples formed at higher temperature. Argon adsorption has evidenced the ultramicroporosity of the materials formed at low temperature, as well as its evolution to secondary porosity with diameters greater than 1.5 nm under more severe hydrothermal treatment.

## Introduction

Recently, hexagonal Micelle-Templated Silicas (MTS) with large surface area (700–900 $m^2\ g^{-1}$), large pore size (5 to 9 nm) and thick walls (3.5 to 5.3 nm) called SBA-15 have been disclosed by Zhao *et al.*[1,2] In these materials, silica is structured by triblock copolymers, *e.g.* $(EO)_{20}(PO)_{70}(EO)_{20}$ (Pluronic P123), in acidic conditions. Syntheses are performed in a temperature range from 35 to 100 °C and provide solids with high thermal and hydrothermal stability. These materials could represent an interesting alternative to large pore MCM-41, synthesized by oil-swelling of quaternary ammonium (CTAB) micelles, which feature walls not thicker than 1 nm.[3] Thin walls are responsible for the low mechanical stability of these MCM-41 materials,[4] the elasticity limits of which increase with the square of the ratio between the wall thickness and the pore opening.[5]

SBA-15 share with MCM-41 a well-defined hexagonal structure. However, the two classes of materials present subtly different adsorption properties. In the case of MCM-41, several methods of pore size measurement, based on the pressure of the desorption step of the nitrogen isotherm, or on the pore volume and the surface area, or on the pore volume and the cell parameter, give very similar results.[6,7] In the case of SBA-15, the pore size of a given solid can vary by a factor of two when evaluated by different methods. For instance, a typical SBA-15 synthesized at 100 °C and calcined at 550 °C, with a cell parameter of 11 nm, a pore volume of 1.17 mL $g^{-1}$ and a BET surface area of 850 $m^2\ g^{-1}$ presents a pore size of 8.9 nm according to the Broekhoff and de Boer (BdB) method (pressure of the isotherm step) and 5.5 nm by the 4V/S method.[8] This discrepancy suggests that the hypotheses at the basis of some measurement methods are not valid in the case of SBA-15, probably due to the presence of microporosity or surface roughness in some samples. The subject has been hotly debated in the last two years.[9–13] The first studies have shown that microporosity could be observed by comparison plots (*t*-plots) for SBA-15 synthesized at 60 °C, but not for SBA-15 synthesized at 100 °C.[10]

In a study devoted to the microporosity of SBA-15, the authors have synthesized SBA-15 samples over a wide range of temperature (35 to 130 °C) and quantitatively evaluated the $N_2$ sorption isotherms and the corresponding *t*-plots to assess the validity of several adsorption models.[8] Large differences have been observed in the adsorption isotherms as a function of the synthesis temperature. The $C_{BET}$ parameter calculated from the BET equation gave negative values for solids prepared between 35 and 90 °C, extremely high positive values for solids prepared between 100 and 110 °C, and a value of 100—the normal value for a hydroxylated silica surface—for the solids prepared at 130 °C. This trend of the $C_{BET}$ parameter indicated that the low-pressure adsorption exceeded the amount expected for monolayer–multilayer adsorption for all samples except for the solids prepared at 130 °C, behavior attributed to the presence of microporosity. The microporous volume was evaluated by a geometrical model taking into account the cell parameter from X-ray diffraction and the mesopore diameter from the pressure of the isotherm step (BdB method), and was shown to be at a maximum for solids prepared between 35 and 80 °C (about 0.3 mL $g^{-1}$, corresponding to nearly a third of the total pore volume), to decrease at higher synthesis temperatures and disappear for the sample prepared at 130 °C. However, *t*-plots indicated the presence of microporosity only in the case of solids prepared between 35 and 90 °C. The failure of *t*-plots to detect any microporosity for the samples prepared between 100 and 120 °C was attributed to the lack of an appropriate reference isotherm for a silica surface pitted by micropore mouths[8] or by the fact that mesopore filling start before the completion of micropore filling.[13] A recent study using the Non-Linear

Density Functional Theory of the adsorption isotherms of SBA-15 has confirmed the presence of microporosity in samples synthesized at 100 °C.[13]

Another feature which renders SBA-15 different from MCM-41 is the presence of connections between parallel mesopores. Mesoporous bridges between pores have been observed by HR-TEM of platinum[14] or carbon[15] replicas and confirmed by direct transmission electron microscopy[16] for solids mostly prepared at 100 °C.

In this article, we focus on some still unanswered questions about the pore system of SBA-15. What are the size and extent of micropores inside the walls of SBA-15? Does the temperature of synthesis affect the connections between mesopores? Is there any relationship between microporosity and mesoporous connections?

## Experimental

### Materials

SBA-15 materials were synthesized according to the procedure described in the literature[2] from batches of 1 g Pluronic P123 [$(EO)_{20}(PO)_{70}(EO)_{20}$, Aldrich], 15 g $H_2O$, 30 g HCl 2 M, 2.1 g tetraethylorthosilicate (TEOS, Aldrich). The mixture was maintained at 35 °C for 24 h and then heated for 24 hours at the synthesis temperature under static conditions in a teflon-lined autoclave.[8] All materials were filtered, washed with deionized water and dried at 80 °C for 24 h. The solids were then calcined in air at 550 °C for 8 h.

The Pt replicas were prepared following the procedure reported in the literature,[17] the calcined SBA-15 silica sample (0.2 g) was loaded with tetraammine platinum(II) nitrate [$Pt(NH_3)_4(NO_3)_2$, Aldrich] (0.16 g) by repeating alternation of the impregnation of aqueous solution ($5 \times 10^{-5}$ mol $L^{-1}$) (solution to sample ratio was 100 mL $g^{-1}$) and drying at 100 °C four times. The Pt-SBA-15 samples were then heated under $H_2$ flow from room temperature to 300 °C for 4 h and maintained at 300 °C for 2 h using a U-tube reactor equipped with two fritted disks. The Pt-SBA-15 samples were then put in a vacuum for 30 min at 300 °C prior to exposure to air at room temperature. The silica framework of Pt-SBA-15 was dissolved completely with HF (10%). The Pt residues were filtered and washed with distilled water. An ethanol dispersion of these Pt samples was dropped onto a TEM grid, and the solvent was dried at room temperature.

### Characterization

Powder X-ray diffraction (XRD) data were obtained on a CGR Thêta-60 diffractometer with an Inel drive, using monochromated Cu Kα radiation.

The adsorption/desorption isotherms of nitrogen or argon at 77 K were measured using a Micromeritics ASAP 2000 instrument. Each sample was outgassed at 250 °C for calcined materials or at 50 °C for as-synthesized materials until a stable static vacuum of $3 \times 10^{-3}$ Torr was reached. The mesopore diameter was calculated from the desorption branch of nitrogen isotherms by the Broekhoff and de Boer (BdB) method, which has been shown to provide reliable results for MCM-41 materials.[7] *t*-Plots were drawn by using as non-microporous reference a MCM-41 with pore size 8.4 nm and surface area 850 $m^2$ $g^{-1}$, prepared in the presence of cetyltrimethylammonium and trimethylbenzene.[3,7]

TEM images were obtained using a Philips CM 20 apparatus operating at 100 keV.

## Results

### XRD

Fig. 1 shows the X-ray diffraction patterns of SBA-15 synthesized at 60, 100, or 130 °C and calcined at 550 °C. The diffraction pattern shows three peaks which can be indexed according to a hexagonal array of mesopores as for MCM-41: reflections due to the diffraction planes (100), (110), (200) are observed. The (110) reflection is more intense for the SBA-15 synthesized at 130 °C which could indicate thinner walls as suggested by Feuston *et al.*[18] for MCM-41. For the SBA-15 synthesized at different temperatures from 35 to 130 °C, the cell parameter of the as-synthesized solids is the same, around 11 nm. After calcination at 550 °C, a shrinking is observed for the SBA-15 synthesized from 35 to 60 °C (9 nm), likely due to incomplete condensation of silica at low temperature. For samples prepared at temperatures from 80 to 130 °C, the cell parameter of calcined samples remains constant at 10.5 nm.

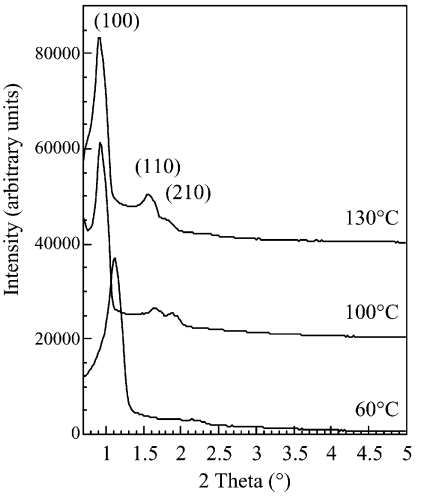


**Fig. 1** XRD pattern of SBA-15 synthesized at 60, 100 and 130 °C and calcined at 550 °C.

### Nitrogen adsorption at 77 K

Fig. 2 shows nitrogen sorption isotherms at 77 K for SBA-15 synthesized from 60 to 130 °C. The isotherms show a sharp step with a hysteresis loop corresponding to the filling of ordered mesopores. The relative pressure of pore filling increases with the temperature of synthesis. The pore diameters evaluated by the BdB method are reported in Fig. 3. A steady increase of the mesopore size with the synthesis temperature is observed beyond 60 °C. The good ordering of the structural mesopores allows us to apply to these materials the geometrical models developed for the pore size evaluation

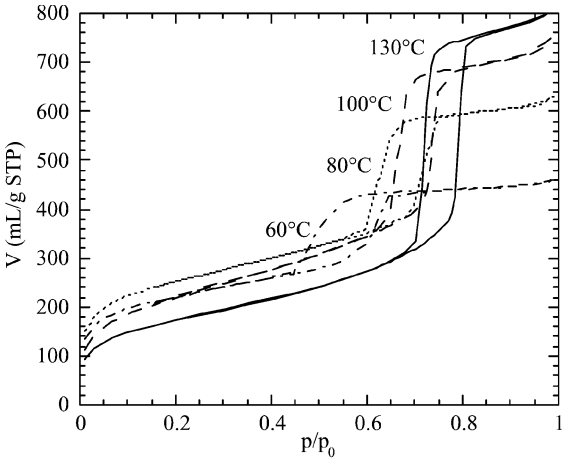


**Fig. 2** Nitrogen adsorption/desorption isotherms at 77 K for SBA-15 synthesized at 60, 80, 100, and 130 °C and calcined at 550 °C.

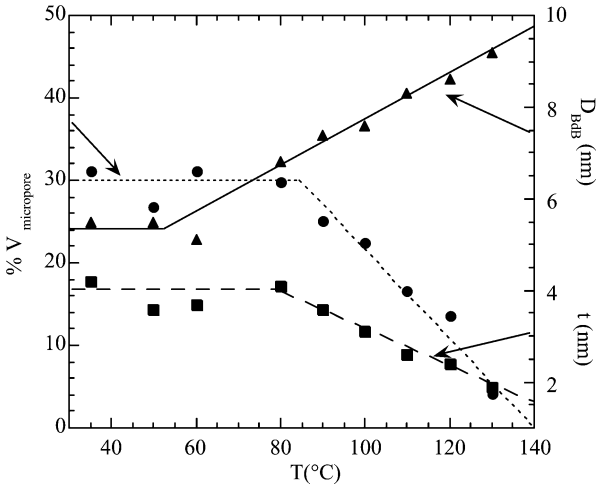


**Fig. 3** Percentage of microporous volume, mesopore diameter and wall thickness of SBA-15 as a function of the synthesis temperature. Pore sizes were calculated by the Broekhoff–de Boer method.

of the MCM-41 honeycombs.[6–8] The mesopore volume can be evaluated from the *a* parameter of the hexagonal cell, the total pore volume and the mesopore size[8] as

$$V_{\mathrm{mes}} = (D_{\mathrm{BdB}}/1.05a)^2[V_{\mathrm{p}} + (1/\rho_{\mathrm{Si}})]$$

with the silica density $\rho_{\mathrm{Si}} = 2.2$. The micropore volume can be evaluated from the difference between the total pore volume and the mesopore volume

$$V_{\mu} = V_{\mathrm{p}} - V_{\mathrm{mes}}$$

and is reported in Fig. 3 as a percentage of the total pore volume. The thickness of the walls between structural mesopores has been measured from the difference between the cell parameter and the equivalent pore diameter, namely, for a hexagonal structure,

$$t = a - 0.95\ D_{\mathrm{BdB}}$$

For samples prepared above 80 °C, the fraction of microporous volume and the wall thickness steadily decrease with the synthesis temperature. The sample prepared at 130 °C shows virtually no microporosity.

### Argon adsorption at 77 K

The argon isotherms at low pressure have been used to characterize the microporosity of SBA-15 samples. Argon as an adsorptive presents some distinct advantages over nitrogen, whose departure from spherical symmetry and strong quadrupole moment result in a blurring of the fine structure of the isotherms.[19] In Fig. 4, the argon adsorption/desorption isotherms at 77 K are reported for SBA-15 samples prepared at 60, 110, and 130 °C.

The low-pressure portion of the isotherms is better evaluated by a *t*-plot in which the amount of adsorbate at a given pressure is related to the amount of adsorbate on a non-microporous reference solid at the same pressure. Any instance of non-linearity in the *t*-plot results from a deviation from the mechanism of monolayer–multilayer adsorption on the reference solid. As long as a multilayer of adsorbate is formed unhindered on the solid surface, the *t*-plot is a straight line passing through the origin. A downward deviation is observed when micropores are present in the solid and an upward deviation indicates the presence of capillary condensation in the pores of the adsorbent. The low-coverage part of the *t*-plot ($t < 0.3$ nm) corresponds to the formation of an adsorbate monolayer (average thickness 0.265 nm[20]) on a non-microporous adsorbent. The *t*-plots of argon adsorption

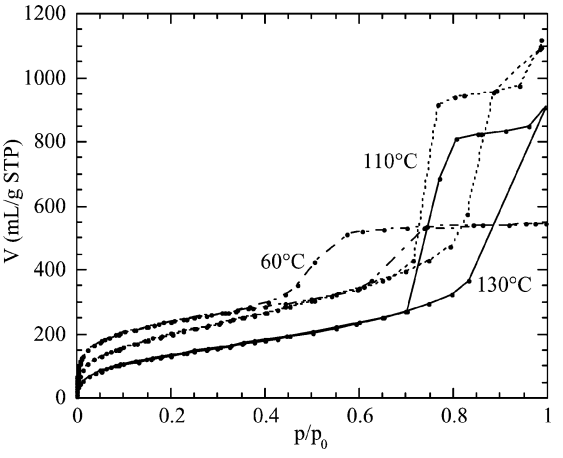


**Fig. 4** Argon adsorption/desorption isotherms at 77 K for SBA-15 synthesized at 60, 110, and 130 °C and calcined at 550 °C.

on SBA-15 prepared at 60, 110, and 130 °C are reported in Fig. 5.

In the case of SBA-15 prepared at 130 °C, the *t*-plot at low coverage is a straight line passing through the origin, indicating that the amount of adsorbate depends on the pressure according to the same laws as in the case of the non-microporous reference. In the case of the SBA-15 samples prepared at lower temperatures, 60 and 110 °C, the slope of the *t*-plots rapidly decreases with coverage. This behavior indicates that adsorption at low pressure does not take place only by monolayer coverage, but also by micropore filling. This deviation from linearity takes place in the same pressure range as zeolite-like ultramicropores (pore diameter < 1 nm). It is worth noting that this ultramicroporosity is uniformly distributed through the mesoporous material and does not correspond to a separated microporous phase. This is witnessed by the thermalisation of the $^{129}$Xe NMR signals, where Xe chemical shifts are shifted to higher values and do not follow the relationship between structural mesopore diameters and Xe chemical shift found for MCM-41, except for SBA-15 materials synthesized at 130 °C which do not contain ultramicropores.[21]

For *t* values higher than 0.15 nm, the SBA-15 sample prepared at 60 °C does not present any further deviation from linearity, indicating that the adsorption continues through a plain multilayer mechanism. However, the SBA-15 samples prepared at 110 and 130 °C present a positive deviation of the *t*-plot for *t* higher than 0.21 nm. This indicates the presence of an additional adsorption mechanism, very likely corresponding to the filling of a secondary porosity with a very broad size distribution. This effect could be related to previous findings of Ryoo *et al.*[12] The authors have modified SBA-15

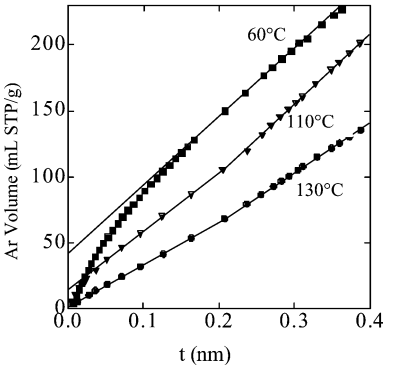


**Fig. 5** Comparison plots of Ar adsorption at 77 K on SBA-15 prepared at 60, 110, 130 °C and calcined at 550 °C. The reference adsorbent was a TMB-swelled MCM-41 calcined at 550 °C.

synthesized at 100 °C by grafting alkylsilanes of different sizes and evaluated the porosity of the resulting solids. They reported the presence of "micropores" (later referred to as complementary pores) with sizes between 1 and 3.4 nm. In MCM-41, the size of mesopores corresponds to six times the $t$ value of the positive deviation. In the case of argon, it seems possible to apply this correlation also to supermicropores ($1 <$ pore diameter $< 2$ nm). Then for SBA-15 synthesized at 110 and 130 °C, a positive deviation of the $t$-plots starting at $t = 0.25$ nm will correspond to a lower limit size of the secondary porosity of 1.5 nm.

### Imaging of Pt replicas of SBA-15

Platinum replicas of SBA-15 have been prepared for calcined samples of SBA-15 synthesized at 60, 100 and 130 °C. In the TEM images, the connections between mesopores can be observed as bridges between their platinum replicas. No significant connections between structural mesopores have been detected for SBA-15 synthesized at 60 °C, the material which presents the greater amount of micropores (Fig. 6). The TEM images are similar to the ones obtained for MCM-41 materials with no connecting bridges between mesopores.[22] Bridges between mesopores have instead been found for SBA-15 synthesized at 100 °C, as reported in the literature,[12,14] as well as for SBA-15 synthesized at 130 °C, which present virtually no microporosity (Fig. 6). The frequency and size of the observed bridges increase with the temperature of synthesis. Bridges of 3–4 nm are observed for the solid prepared at 100 °C and bridges of 4–5 nm for SBA-15 synthesized at 130 °C. These values are very close to the length of a side of the pore, if represented with a hexagonal section. The distance between bridges is larger than 9 nm and no order in the distribution of connections can be observed. This secondary porosity due to mesoporous bridges will represent less than 6% of the total pore volume, this volume is included in our calculation of microporous volume in Fig. 3.

The method of preparation of the Pt replicas does not guarantee the preservation of pores smaller than 2 nm during the decomposition of the platinum complexes. As a consequence, the presence of connections at the microporous scale can not be directly excluded by the absence of bridges in the Pt replicas.

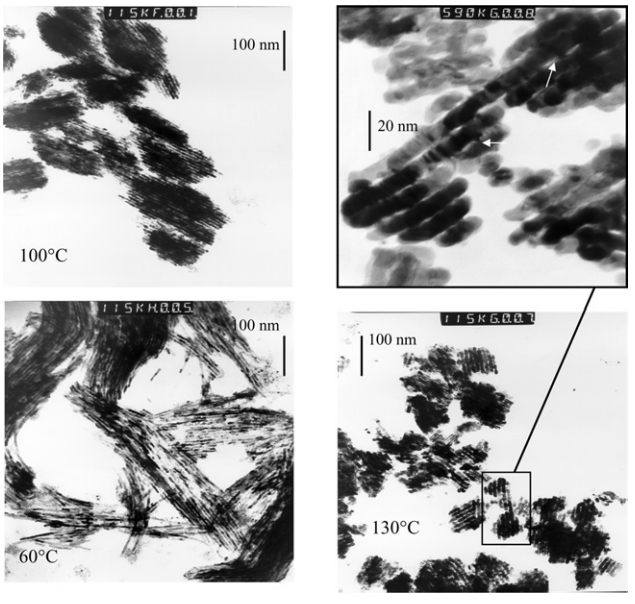


**Fig. 6** TEM images (×230 000) of a platinum replica of SBA-15 synthesized at 60, 100 and 130 °C. Magnification (×1 180 000) of a platinum replica of SBA-15 synthesized at 130 °C, arrows showing connections between the main mesopores.

## Discussion

The complexity of the pore structure of SBA-15 can be easily evidenced if these materials are compared with MCM-41. The structure of MCM-41 is neatly described as a honeycomb of hexagonal mesopores[23] separated by continuous silica walls. In the case of such a simple structure, plain geometrical calculations allow us to determine the surface area and the pore volume of the materials from the cell parameter and the wall thickness (Fig. 7):[5,24]

$$S = 4 \times 10^3(1 - t/a)/[t\rho_{Si}(2 - t/a)]$$

$$V = a(1 - t/a)^2/[t\rho_{Si}(2 - t/a)]$$

with $t$ and $a$ in nm.

These expressions give consistent results for MCM-41, by using the proper BET surface area[7] and pore volume determined by nitrogen adsorption and $t$-plot analysis. In the instance of SBA-15 synthesized at low temperature, for a cell parameter of 10.5 nm and wall thicknesses of 3–5 nm, a hexagonal model would predict surface areas around 200–300 $m^2$ $g^{-1}$, instead of the observed 600–900 $m^2$ $g^{-1}$, and pore volumes lower than 0.5 mL $g^{-1}$ instead of the observed 1 mL $g^{-1}$.[8] It is clear that, albeit the XRD indicates a neat hexagonal order of the material, the adsorption data (surface areas 600–900 $m^2$ $g^{-1}$ and pore volumes 0.8–1.3 mL $g^{-1}$) do not correspond to a hexagonal honeycomb structure with continuous silica walls. Patently some adsorption takes place outside the structural hexagonal mesopores.

The comparison of the data for SBA-15 prepared at different temperatures allows us to differentiate, in addition to the structural mesopores, two kinds of complementary porosity, an ultramicroporosity (pore size $< 1$ nm)[25] and a secondary porosity with a very broad pore size distribution between 1.5 nm and 3–5 nm (depending on synthesis temperature). The presence of zeolite-like ultramicropores, with a size smaller than a threshold situated not far from 1 nm, is clearly indicated by the $t$-plot of argon adsorption and is strictly related to the already observed anomaly of the $C_{BET}$ parameter of the BET equation.[8] The maximum extent of ultramicroporosity is observed in samples prepared at temperatures not higher than 80 °C. When the synthesis system is treated at higher temperature, the ultramicroporous volume decreases and virtually disappears for samples prepared at 130 °C.

The decrease of the ultramicroporosity is accompanied by the appearance in the $t$-plot analysis of the secondary porosity starting in the supermicroporosity range, as indicated by the positive deviation of the $t$-plot of argon adsorption which extends without discontinuity beyond the threshold of 2 nm into the field of mesopores. The fraction with larger pore size of the secondary porosity can be related to the mesoporous connections evidenced by the microscopy of the platinum replicas.

Are ultramicroporosity and secondary porosity related? The simultaneous disappearing of ultramicroporosity and appearing of secondary porosity suggests a possible transformation of the former into the latter during the thermal treatment of the synthesis system. It has been earlier suggested that structural mesopores can be connected through micropores.[8,16] In the case of supermicroporosity coming from the secondary porosity, strictly related to the mesoporous connections evidenced by platinum replicas, this statement seems to be well-supported. The case for ultramicroporous connections is more complex. They cannot be observed by microscopy of platinum replicas, but this is not a clear disproof of their presence: such tiny platinum bridges could easily be unstable under the conditions in which the replicas have been prepared. However, the presence of ultramicroporous connections in the samples prepared at low temperature is deemed unlikely by these authors,

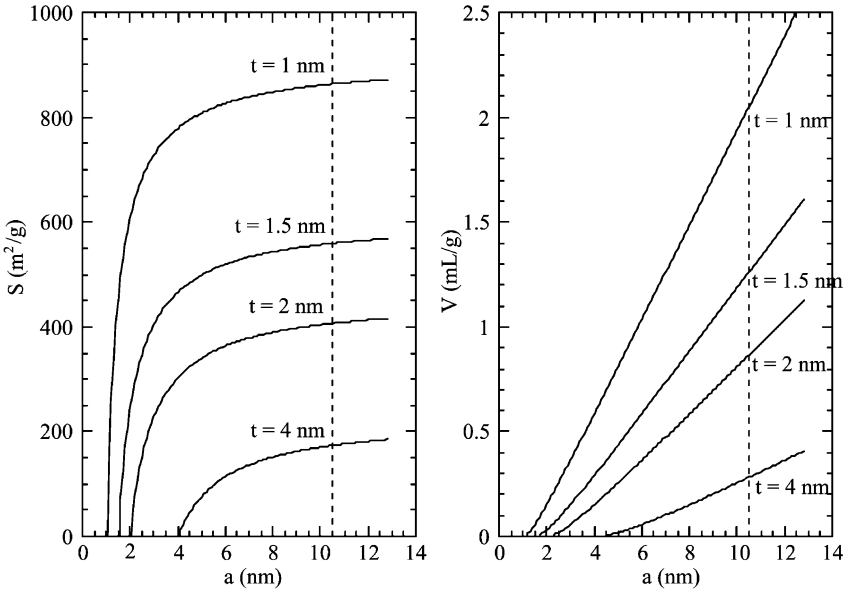


**Fig. 7** Theoretical volume and surface area of a hexagonal honeycomb structure with hexagonal pores as a function of the wall thickness, *t*, and cell parameter, *a*. The dashed line indicates the cell parameter for SBA-15 materials.

on the basis of some hypotheses on the mechanism of formation of these materials.

The presence of ultramicropores in SBA-15 walls can be explained by the micellar behavior of non-ionic surfactants, which has been extensively studied in the absence of silica.[26] Non-ionic micelles in water are surrounded by a corona of hydrated polyethylene oxide (PEO) chains protruding by nearly 1 nm from the average micelle surface.[27] When an isotropic micellar solution is formed, the repulsion between opposite combs of hydrated PEO chains takes the micelles to a distance of at least 3–4 nm. PEO chains pertaining to adjacent micelles do not share their hydration shells (Fig. 8). The situation changes when temperature increases: water becomes a less effective solvent, the PEO chains withdraw on the surface of the micelle and a net intermicellar attraction arises from PEO–PEO interactions between adjacent micelles. At the cloud point (85 °C in the case of Pluronic 123), micelles interact strongly enough to form aggregates which separate from the diluted solution.

The evolution of SBA-15 with the synthesis temperature closely corresponds to this pattern. In all syntheses, the first step is a day-long aging at 35 °C, during which the presence of silica prompts the formation of a composite mesophase at surfactant concentrations at which only an isotropic solution[28] is present in the absence of silica (see Fig. 9). Ordered SBA-15 materials are the result of the restructuring of this precursor mesophase formed at low temperature. If the precursor mesophase is not allowed to form (no pre-aging step at 35 °C) and the synthesis temperature is raised immediately, the solid formed will be disordered, with a broad pore size distribution and hystereses indicative of restrictions at the mouth of the pores.

SBA-15 materials formed at the lowest temperatures are expected to fairly represent the properties of the precursor mesophase. The wall thickness of the materials formed at temperatures not higher than 60 °C, about 4 nm, corresponds to the minimum distance between hydrated micelles in water. This is strongly suggestive of a mechanism of impregnation of the intermicellar space by the silica precursors, in which the observed ultramicroporosity would be templated by the protruding PEO chains. If the silica walls should reproduce the topology of the hydration shells of the PEO chains in water, no microporous bridges should be expected between adjacent micelles at low temperature.

When the precursor mesophase formed at 35 °C is heated at temperatures higher than 80 °C, its fine structure (corresponding to micellar solution templating) is not preserved: the size of the structrural mesopores increases, the thickness of the walls decreases, the ultramicroporosity disappears and a pore-bridging secondary porosity appears. The temperature at which these phenomena begin to take place is very close to the cloud point of the surfactant, which indicates a lower solvation of the PEO chains. Interestingly, silica-embedded micelles behave

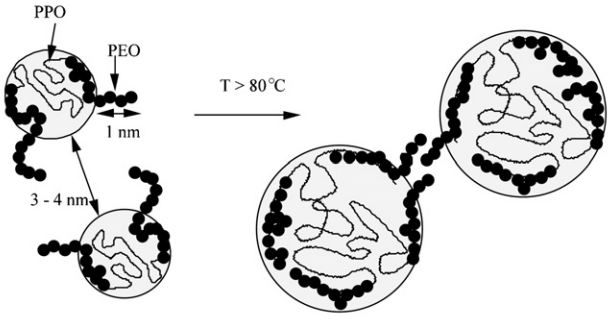


**Fig. 8** Schematic representation of micelle dehydration upon temperature.

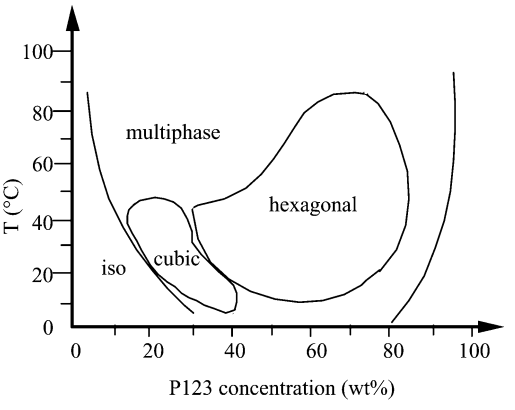


**Fig. 9** Phase diagram of P123, $EO_{20}PO_{70}EO_{20}$, reproduced with permission from ref. 28.

like micelles in water: the disappearance of ultramicroporosity parallels the disappearance of PEO fingers. PEO chains become a less efficient template for silica, and this effect corresponds to a weaker interaction between PEO and silica. The reduced strength of the PEO–silica interaction at higher temperature is evidenced by the easier extraction of surfactant by water washing after the synthesis: nitrogen isotherms at 77 K of as-synthesized SBA-15 indicate that water washing has only liberated 5% of the porosity for SBA-15 synthesized at 60 °C, whereas 50% of porosity is recovered by simple water washing for SBA-15 synthesized at 130 °C.

The weakest interaction between PEO and silica destabilizes the corona of PEO-templated ultramicroporous silica which surrounded the micelles of the precursor mesophase. A phase separation of PEO and silica takes place at the nanometer scale, bringing about an increase of the size of the structural mesopores and a densification of the silica walls. It is interesting to observe that the cell parameter of the hexagonal structure remains virtually constant upon the hydrothermal treatment, just as the evolution of the precursor mesophase with temperature took place by redistribution of the organic volume inside a close microreactor. The densification of the silica walls corresponds to an important decrease of the wall thickness, which parallels the decrease of microporous volume (Fig. 3). The process probably takes place in a haphazard way, with the opening of local gaps in the walls, which are at the origin of the secondary porosity and of the bridges between structural mesopores.

The opening of bridges between the structural mesopores of SBA-15 synthesized at $T > 80$ °C, thus in the system non-ionic surfactant–silica–water, seems to parallel the connections between micelles at the cloud point in the system non-ionic surfactant–water. Although the driving force is undoubtedly the same, the weaker interaction between the micelle and its solvent, the differences between the two systems provide information on the role of the inorganics in the formation of composite mesophases. The increase of the mesopore size with temperature does not have a clear-cut equivalent in the water–surfactant systems. The partial dehydration of the PEO chains could be expected to bring about a decrease of the area/volume ratio of the micelles and an increase of the aggregation number of the non-ionic surfactants, in a similar way as the increase of ionic strength corresponds to an increase of the aggregation number of the ionic surfactants. However, experimental evidence does not show such general behavior for non-ionic surfactants.[26] The variation of the thickness of the interface layer, a property somehow difficult to characterize, compensates the changes of the interface between the micelle and the solution, and no consistent trends of the aggregation number are observed over a wide range of temperature variation. Moreover, the role of residual water in the formation of composite mesophases is far from being elucidated.

Some caveats should also be formulated about the interpretation of the adsorption data. If the ultramicroporosity of SBA-15 is indeed templated by PEO fingers protruding from the micellar surface, the maximum depth of micropores should be expected to be about 1 nm. Micropores with a depth/diameter ratio about one are at the borderline of surface roughness, and well-defined adsorption mechanisms do not yet exist for this kind of porosity. This shortcoming is probably at the basis of the important difference between the ultramicropore volume as evaluated by the argon *t*-plot and the micropore volume estimated by nitrogen adsorption.[8]

However, the data of argon adsorption at low pressure provide a useful addition to the data of nitrogen adsorption, and allow us to improve their interpretation. For instance, the *t*-plot of the nitrogen adsorption data did not provide evidence for any microporosity for the samples prepared at 100 or 110 °C, despite the fact that the increased surface area of these samples strongly suggested the presence of pores smaller than the structural porosity.[8] The *t*-plot of argon adsorption for the sample prepared at 110 °C (Fig. 5) is characterized by a negative deviation due to the ultramicroporosity and a positive deviation due to distributed supermicroporosity–mesoporosity. If the *t*-plot is drawn only for coverage higher than monolayer, as is the case in the high-coverage nitrogen *t*-plot, these deviations compensate one another and the extrapolation of the *t*-plot passes through the origin, despite the presence of ultramicroporosity. In some way, the presence of a distributed porosity is at the origin of the spurious linearity of the nitrogen *t*-plot.

## Conclusions

Imaging of the platinum replica of the porous structure and low-pressure argon adsorption allowed us to elucidate the complicated porous structure of SBA-15. These techniques enabled us to draw a coherent picture of the evolution of the SBA-15 precursor mesophase as a function of the synthesis temperature. TEM of the platinum replicas has been unable to show bridges between the structural mesopores of SBA-15 synthesized at low temperature, whereas mesoporous bridges are clearly observed for samples formed at higher temperature. Argon adsorption has evidenced the ultramicroporosity of the materials formed at low temperature, as well as its evolution to secondary porosity with diameters greater than 1.5 nm under more severe hydrothermal treatment.

The complex, synthesis-dependent topology of the SBA-15 pore system can be depicted in the following way: the precursor mesophase and the SBA-15 synthesized below 80 °C feature ultramicroporous silica walls nearly 4 nm thick between structural mesopores with a diameter close to 5 nm. This

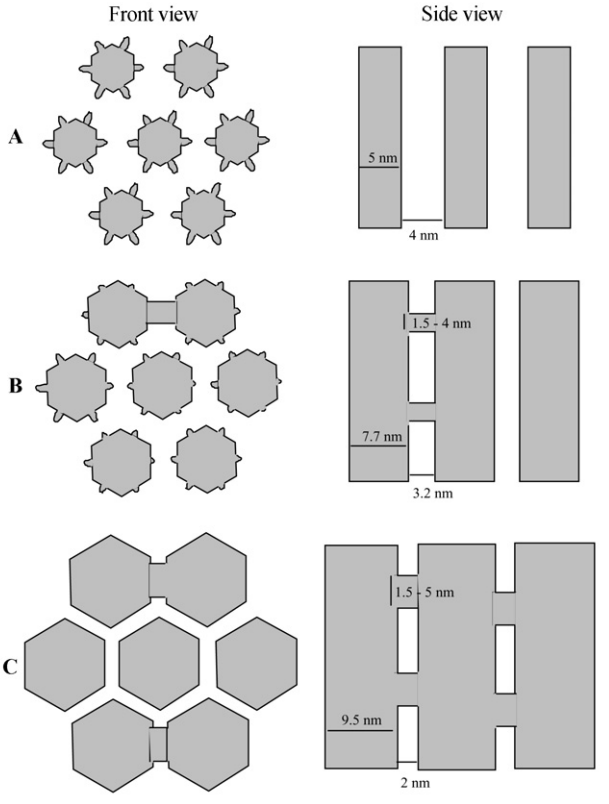


**Fig. 10** Schematic representation of SBA-15 synthesized (A) between 35 and 60 °C showing micropores and no connection between mesopores, (B) around 100 °C showing micropores and connections between mesopores and (C) at 130 °C showing no micropores but connections between mesopores.

microporosity is the result of silica templating by PEO fingers forming a corona around each micelle. Very likely, the parallel mesopores are not connected through the ultramicroporous corona (Fig. 10). When the synthesis temperature is higher than 80 °C, the precursor mesophase is gradually modified by a decrease in the strength of the interaction between the surfactant and its environment and by a densification of silica inside the walls. The mesopore size increases, the wall thickness decreases, and the collapse of the ultramicroporosity brings about the formation of secondary porosity, spanning from supermicropores to small mesopores which represent bridges between adjacent mesopores. The solid formed at 130 °C is well representative of a final stage of this evolution, with mesopores of more than 9 nm separated by 2 nm thick silica walls which present no ultramicroporosity. A secondary porosity spanning from 1.5 to 5 nm forms bridges between the structural mesopores.

The existence of ultramicroporosity which disappears with hydrothermal treatment ($T > 80$ °C) and of secondary porosity bridges between pores which appears with temperature can be expected to be a general feature for all MTS synthesized using surfactants with oligomeric ethylene oxide chains as the hydrophilic part.

## References


1 D. Y. Zhao, J. L. Feng, Q. S. Huo, N. Melosh, G. H. Fredrickson, B. F. Chmelka and G. D. Stucky, *Science*, 1998, **279**, 548.
2 D. Y. Zhao, Q. S. Huo, J. L. Feng, B. F. Chmelka and G. D. Stucky, *J. Am. Chem. Soc.*, 1998, **120**, 6024.
3 D. Desplantier-Giscard, A. Galarneau, F. Di Renzo and F. Fajula, *Stud. Surf. Sci. Catal.*, 2001, **135**, 205.
4 D. Desplantier-Giscard, O. Collart, A. Galarneau, P. Van der Voort, F. Di Renzo and F. Fajula, *Stud. Surf. Sci. Catal.*, 2000, **129**, 665.
5 A. Galarneau, D. Desplantier-Giscard, F. Di Renzo and F. Fajula, *Catal. Today*, 2001, **68**, 191.
6 N. Coustel, F. Di Renzo and F. Fajula, *J. Chem. Soc., Chem. Commun.*, 1994, 967.
7 A. Galarneau, D. Desplantier, R. Dutartre and F. Di Renzo, *Microporous Mesoporous Mater.*, 1999, **27**, 297.
8 A. Galarneau, H. Cambon, F. Di Renzo and F. Fajula, *Langmuir*, 2001, **17**, 8328.
9 V. B. Fenelov, A. Y. Derevyankin, S. D. Kirik, L. A. Solovyov, A. N. Shmakov, J.-L. Bonardet, A. Gedeon and V. N. Romannikov, *Microporous Mesoporous Mater.*, 2001, **44–45**, 33.
10 M. Kruk, M. Jaroniec, C. H. Ko and R. Ryoo, *Chem. Mater.*, 2000, **12**, 1961.
11 M. Impéror-Clerc, P. Davidson and A. Davidson, *J. Am. Chem. Soc.*, 2000, **122**, 11 925.
12 R. Ryoo, C. H. Ko, M. Kruk, V. Antochshuck and M. Jaroniec, *J. Phys. Chem. B*, 2000, **104**, 11 465.
13 P. I. Ravikovitch and A. V. Neimark, *J. Phys. Chem. B*, 2001, **105**, 6817.
14 Z. Liu, O. Terasaki, T. Ohsuna, K. Hiraga, H. J. Shin and R. Ryoo, *Chem. Phys. Chem.*, 2001, **4**, 229.
15 H. J. Shin, R. Ryoo, M. Kruk and M. Jaroniec, *Chem. Commun.*, 2001, 349.
16 J. Fan, C. Yu, L. Wang, B. Tu, D. Zhao, Y. Sakamoto and O. Terasaki, *J. Am. Chem. Soc.*, 2001, **123**, 12 113.
17 (*a*) C. H. Ko and R. Ryoo, *Chem. Commun.*, 1996, 2467; (*b*) R. Ryoo, J. M. Kim, C. H. Ko and H. J. Shin, *J. Phys. Chem.*, 1996, **100**, 17 718; (*c*) H. J. Shin, C. H. Ko and R. Ryoo, *J. Mater. Chem.*, 2001, **11**, 260.
18 B. P. Feuston and J. B. Higgins, *J. Phys. Chem.*, 1994, **98**, 4459.
19 J. H. de Boer, B. G. Linsen and T. J. Osinga, *J. Catal.*, 1965, **4**, 643.
20 D. A. Payne, K. W. Sing and D. H. Turk, *J. Colloid Interface Sci.*, 1973, **43**, 287.
21 A. Galarneau, H. Cambon, T. Martin, L.-C. De Menorval, D. Brunel, F. Di Renzo and F. Fajula, *Stud. Surf. Sci. Catal.*, 2002, **141**, 395.
22 Z. Liu, Y. Sakamoyo, T. Ohsuna, K. Hiraga, O. Terasaki, C. H. Ko, H. J. Shin and R. Ryoo, *Angew. Chem., Int. Ed.*, 2000, **39**, 3170.
23 M. F. Ottaviani, A. Galarneau, D. Desplantier-Giscard, F. Di Renzo and F. Fajula, *Microporous Mesoporous Mater.*, 2001, **44–45**, 1.
24 F. Di Renzo, A. Galarneau, P. Trens, N. Tanchoux and F. Fajula, *Stud. Surf. Sci. Catal.*, 2002, **142**, 1057.
25 S. J. Gregg and K. S. W. Sing, in *Adsorption, Surface Area and Porosity*, Academic Press, London, 1982, p. 244.
26 C. Booth and D. Attwood, *Macromol. Rapid Commun.*, 2000, **21**, 511.
27 J. N. Israelachvili and H. Wennerström, *J. Phys. Chem.*, 1992, **96**, 520.
28 G. Wanka, H. Hoffmann and W. Ulbricht, *Macromolecules*, 1994, **27**, 414.